Available online at www.sciencedirect.com
ScienceDirect
Journal of Power Sources 175 (2008) 137–144
JOURNAL OF POWER SOURCES
www.elsevier.com/locate/jpowsour

Formation of $Ce_{0.8}Sm_{0.2}O_{1.9}$ nanoparticles by urea-based low-temperature hydrothermal process

Ming-Yao Cheng [a], Ding-Han Hwang [a], Hwo-Shuenn Sheu [b], Bing-Joe Hwang [a,b,*]

[a] *Nano-electrochemistry Laboratory, Department of Chemical Engineering, National Taiwan University of Science and Technology, Taipei 106, Taiwan, ROC*
[b] *National Synchrotron Radiation Research Center, Hsinchu 300, Taiwan, ROC*

Received 9 July 2007; received in revised form 3 September 2007; accepted 4 September 2007
Available online 11 September 2007

Abstract

The synthesis and formation mechanism of the nano-sized $Ce_{0.8}Sm_{0.2}O_{1.9}$ particles prepared by a urea-based low-temperature hydrothermal process was investigated in this study. From ex situ X-ray diffraction and induced coupled plasma-atomic emission spectroscopy investigations, it was found that large quantities of cerium hydroxide co-precipitated with some samarium hydroxide at the initial stage of the hydrothermal process. The remaining Sm^{3+} ions in the solutions were further hydrolyzed and deposited on the surface of the cerium hydroxide-rich precipitates to form a core–shell-like structure. During the hydrothermal process, the core–shell-like structure transformed to a single cubic fluorite phase which is due to the incorporation of the deposited samarium hydroxide into the cerium oxide-rich core. Further, the average grain size of the synthesized nanocrystalline $Ce_{0.8}Sm_{0.2}O_{1.9}$ was reduced with increasing the urea concentration in the solution. The density of the disk prepared with the synthesized $Ce_{0.8}Sm_{0.2}O_{1.9}$ powders was found to increase with a decrease in the grain size of $Ce_{0.8}Sm_{0.2}O_{1.9}$. The existence of SO_4^{2-} anions in the SDC powders prepared at low-urea concentration may result in the SDC disks with low density due to their decomposition during sintering process.

Keywords: $Ce_{0.8}Sm_{0.2}O_{1.9}$; Solid oxide fuel cell; Solid electrolyte; Nanoparticles; LT-hydrothermal; Urea

1. Introduction

Cerium oxide-based materials were widely studied in decades due to their unique properties. Substitution of cerium by dopants with valence different from that of cerium (4+) in cerium oxide crystalline structures leads to extrinsic oxygen vacancies. Therefore, oxygen could be extracted from or inserted into the lattices of cerium oxide-based materials at oxygen lean or oxygen-rich atmosphere, respectively. It results in wide varieties of their applications in industries [1–4].

Depending on dopant types, the doped cerium oxides could behave as either oxygen ionic conductors or ionic–electronic mixed conductors. Sm^{3+}-, Gd^{3+}- and Y^{3+}-doped cerium oxides with high-ionic conductivities have been considered as solid electrolyte materials for solid oxide fuel cells (SOFCs) [5–14], especially for intermediate temperature SOFC (IT-SOFC, 600–800 °C) [11–14]. For example, $Ce_{0.8}Sm_{0.2}O_{1.9}$ shows high-ionic conductivity of around 0.1 S cm^{-1} which is three times higher than that of the conventional 8YSZ (8 mol% yttria stabilized zirconia, 3×10^{-2} S cm^{-1}) at 800 °C [9,14,15].

A membrane-electrode-assembly (MEA) of SOFC composes of an electrolyte material and two porous electrodes. To reduce the differences of the thermal expansion coefficients between electrode and electrolyte, electrodes are usually constituted by active materials for redox reactions and the corresponding electrolyte materials. In addition, with the introduction of electrolyte materials into electrodes, the length of three-phase boundaries (TPBs) is increased. TPB is the region where redox reaction takes place. The higher amounts the TPBs are,

* Corresponding author at: Nano-electrochemistry Laboratory, Department of Chemical Engineering, National Taiwan University of Science and Technology, Taipei 106, Taiwan, ROC. Tel.: +886 2 27376624; fax: +886 2 27376644.
E-mail address: bjh@mail.ntust.edu.tw (B.-J. Hwang).

0378-7753/$ – see front matter © 2007 Published by Elsevier B.V.
doi:10.1016/j.jpowsour.2007.09.005

the better the performance is. During MEA fabrication, high-temperature treatment is required for the better adhesion of electrode–electrolyte interface. Better electrode network with good electronic and ionic conductivity is also achieved by high-temperature treatment. Unfortunately, the length of TPBs is reduced because serious sintering of the active electrode materials may occur during the high-temperature treatment. Therefore, reduction of heat-treatment temperature during MEA fabrication is of great importance for the improvement of the cell performance of SOFCs.

Nano-sized materials possess better sintering ability than bigger ones. Dimension of the materials is determined by the synthesis route. Various routes have been utilized for preparing electrolyte materials in the literatures, such as solid-state reaction, co-precipitation, sol–gel route and micro-emulsion [16], etc. Most of the methods involve a heat-treatment process to obtain materials with desired crystalline structure. However, the heat treatment would increase the crystalline size of the resulting materials. In hydrothermal routes, materials with desired crystalline structure can be achieved without high-temperature treatment. Further, nano-sized materials are also obtained. Greenblatt and co-workers synthesized a series of lanthanide doped cerium oxide nanoparticles with uniform particle size distribution by a hydrothermal route [3,17–19]. The average crystalline sizes of the synthesized doped cerium oxides were lower than 100 nm, depending on the types and concentrations of the dopants in the doped cerium oxides (33–40 nm for $Ce_{1-x}Tb_xO_{2-\delta}$ [3], 35–50 nm for $Ce_{1-x}Pr_xO_{2-\delta}$ [17], 7–14 nm for $Ce_{1-x}Sm_xO_{2-x/2}$ [18], 41–68 nm for $Ce_{1-x}Gd_xO_{2-\delta}$ [19]). Even $Ce_{1-x}Fe_xO_2$, which is difficult to be synthesized with other methods, could be achieved by using a hydrothermal route with the crystalline size distribution of 12–15 nm [20].

Cerium oxide synthesized by a urea-based hydrothermal process has been reported in the literatures [21–25]. Hydrolysis of urea produces hydroxyl ions to increase the pH value of the solution, subsequently cerium oxide is precipitated. Nano-sized natures of the synthesized CeO_2 particles were revealed with uniform distribution in dimension. It was shown that the quantity of the nuclei and the size of the synthesized CeO_2 were influenced significantly by the concentration of the urea [25]. However, to the best of our knowledge, the doped CeO_2 material synthesized by a low-temperature urea-based hydrothermal method has never been seen in the literatures.

In this study, the formation of $Ce_{0.8}Sm_{0.2}O_{1.9}$ nanoparticles prepared by a urea-based low-temperature hydrothermal (denoted as LT-hydrothermal later) process was investigated. Better understanding of the formation mechanism of $Ce_{0.8}Sm_{0.2}O_{1.9}$ nanoparticles by urea-based LT-hydrothermal process was provided. The properties of the synthesized $Ce_{0.8}Sm_{0.2}O_{1.9}$ were also investigated.

2. Experimental

2.1. Synthesis of $Ce_{0.8}Sm_{0.2}O_{1.9}$ nanoparticles

$Ce(SO_4)_2{\cdot}4H_2O$, $Sm(NO_3)_3{\cdot}6H_2O$ and urea were purchased from Acros and used without further purification. De-ionized water was used in all experiments. The $Ce(SO_4)_2$ solution was prepared by dissolving 8×10^{-3} mol $Ce(SO_4)_2{\cdot}4H_2O$ into 100 ml water with stirring. 0.02 M $Sm(NO_3)_3{\cdot}6H_2O$ solution of 100 ml was then mixed with the $Ce(SO_4)_2$ solution. Meanwhile, the yellow and transparent solution was turned into milk-white. Later, corresponding amount of urea was added to the solution with stirring until totally dissolved. The solution was then poured into a round bottom flask with water-cooled condenser and heated in a glycerol bath at 100 °C. The temperature was held until the solution was changed from originally milky-white to light orange. The light orange precipitates were collected and washed with distilled water for several times and then were spray-dried at 95–100 °C or dried naturally in the atmosphere in some cases for characterization.

For preparation of the electrolyte disks, 0.1 g $Ce_{0.8}Sm_{0.2}O_{1.9}$ nanoparticles were uni-axial pressed with as oil press in 1 metric tonnes cm^{-2}. The furnace temperature was raised with a heating rate of 5 °C min^{-1} up to 1000 °C and 2 °C min^{-1} until 1400 °C and maintained for 5 h.

2.2. Characterization

ICP-AES (Kontron S-35) was performed for analysis of the concentrations of Ce^{4+} and Sm^{3+} ions in the solution. The solution was sampled at the required time until end point. The sampled solutions were centrifuged for separating solid precipitates from liquid, which was submitted to analyze the Ce^{4+} and Sm^{3+} concentrations. FTIR spectra (Digilab FTS-3500) were recorded by accumulating 128 scans over the wave number range of 4000–400 cm^{-1}. For the sample preparation, proper amount of materials was taken and well mixed with KBr and pressed into disks. The spectra of the commercial CeO_2 and Sm_2O_3 powders were also taken for comparison. TEM analysis of the synthesized $Ce_{0.8}Sm_{0.2}O_{1.9}$ nanoparticles was characterized by a JEOL JEM-1010 transmission electron microscope with an accelerating voltage of 80 kV. The powders were added in ethanol with ultrasonic treatment. Then the solution was immediately sampled by a micropipette and dropped onto a carbon coated Cu grid. The Cu grids were then placed in an oven at 70 °C for removing the solvent.

To identify the crystalline structures of the formed precipitates during the developed process, ex situ XRD was performed by using synchrotron radiation source (BL17A, NSRRC, Hsinchu, Taiwan) with an X-ray wavelength of 1.32633 Å (9.3 keV) and 1.5 mm × 0.5 mm in beam size. The apparatus for the hydrothermal process was the same as described in Section 2.1. Small amounts of the precipitates were taken out and placed into a designed Teflon holder with Kapton® tape window. The X-ray beam went through the holder and the diffraction patterns were recorded with image plates. Each pattern was collected for 10 min. A in-house Rigaku X-ray diffractometer was utilized with a Cu Kα radiation source. The data were collected from 20° to 60° in 2θ scale with a scan rate of 2° min^{-1}. The peak positions in the gained XRD pattern were calibrated by silicon powders. The lattice parameters were calculated by the calibrated peak positions of the synthesized powders.

Morphologies of the sintered disks were observed by FESEM (JSM-6500F, JEOL) with the accelerating voltage of 15 kV. The densities of the prepared disks were measured by a densimeter (MD-200S, MIRAGE).

3. Results and discussion

Formation of $Ce_{0.8}Sm_{0.2}O_{1.9}$ nanoparticles was conducted by an urea-based LT-hydrothermal process with urea concentration from 0.2 to 2.0 M. The time-dependent pH value of the solution was recorded during the hydrothermal process, as shown in Fig. 1. The pH value of the original solution was around 1.5 and increases slightly with urea concentration. It was found that the pH value decreases slightly with time at the beginning but increases abruptly after the incubation period. The incubation time decreases with increasing urea concentration. The following reactions took place in the dissolved $Ce(SO_4)_2$ and $Sm(NO_3)_3$ solutions.

$$[Ce(H_2O)_n]^{4+} + yH_2O \rightarrow [Ce(OH)_y(H_2O)_{n-y}]^{(4-y)+} + yH_3O^+ \quad (1)$$

$$[Sm(H_2O)_m]^{3+} + zH_2O \rightarrow [Sm(OH)_z(H_2O)_{n-z}]^{(3-z)+} + zH_3O^+ \quad (2)$$

Both reactions (1) and (2) will generate H^+ ions and result in the decrease of the pH of the solution. However, the decomposition of urea at the temperature higher than 70 °C would release cyanate ions which are further hydrolyzed to form ammonium ions, resulting in the consumption of H^+ ions in an acidic solution [25]:

$$H_2N\text{–}CO\text{–}NH_2 \leftrightarrow NH_4^+ + OCN^- \quad (3)$$

$$OCN^- + 2H^+ + H_2O \rightarrow CO_2 + NH_4^+ \quad (4)$$

Therefore the hydrolysis of urea consumed H^+ ions and caused the increase of pH. The pH of the solution was slightly decreased or almost remained constant at the beginning period, indicating that the proton generation rate is slightly higher or similar compared to the proton consumption rate. After the induction period, the pH increases dramatically, implying that the proton consumption rate is much faster than the proton generation rate. In the basic solution, the cyanate ions will react with OH^- and produce ammonia. The reaction can be written as

$$OCN^- + OH^- + H_2O \rightarrow {CO_3}^{2-} + NH_3 \quad (5)$$

The condensation reaction following after the reactions (1) and (2) happened during the hydrothermal process.

$$[Ce(OH)_y]^{(4-y)+} \rightarrow [CeO_2]_z[Ce_{1-z}(OH)_{y-4z}] + 2zH_2O \quad (6)$$

$$[Sm(OH)_y]^{(3-y)+} \rightarrow [Sm_2O_3]_z[Sm_{1-2z}(OH)_{y-6z}] + 3zH_2O \quad (7)$$

During the hydrothermal process, the composition of the solution was monitored by ICP-AES, as shown in Fig. 2. From Fig. 2(a), the concentration of Ce^{4+} ions in solution was only 3.2% of the total Ce^{4+} value (stock concentration: 5604.8 ppm, 0.08 M $Ce(SO_4)_2$ solution) at the beginning, indicating that the hydrolysis reaction of the Ce^{4+} ions took place and was followed by the precipitation reaction immediately. For Sm^{3+} ions, the initial concentration was 73% of its stock composition (1504 ppm, 0.02 M $Sm(NO_3)_3$ solution), as shown in Fig. 2(b). It implies that 27% of Sm^{3+} ions were incorporated into the $Ce(OH)_4$ precipitates via a co-precipitation process at very early stage even through the pH of the solution was still lower than the required pH for the hydrolysis of Sm^{3+} ions. Then the concentration of Sm^{3+} ions decreased gradually in 40 min although the pH is still lower than the original pH of the $Sm(NO)_3$ solution in which the precipitation of Sm^{3+} ions is not observed in a pure Sm^{3+} solution. It implies that the precipitation of Sm^{3+} ions can occur before reaching the solubility constant in the bulk aqueous solution via a co-precipitation process or due to the existence of precipitates [26]. After 60 min, the concentration of Sm^{3+} ions drops dramatically. It was believed that the decrease of the Sm^{3+} concentration was due to strong hydrolysis and precipitation of Sm^{3+} ions by the increase of the pH in the solution. After 120 min, the concentration of Sm^{3+} ions was close to zero, indicating the precipitation of Sm^{3+} was complete after 120 min at the urea concentration of 0.8 M. The time required to complete the precipitation of Ce^{4+} and Sm^{3+} ions increases with a decrease in urea concentration.

The time-resolved XRD patterns for the precipitates obtained at various stages were shown in Fig. 3. First, the wavelength of the obtained XRD patterns was transformed to the wavelength of Cu Kα. When the $Sm(NO_3)_3$ with $Ce(SO_4)_2$ solutions were mixed together (0 h), the precipitates formed immediately. Hirano et al. [24] have proposed that $Ce(OH)_4$ was formed at the beginning, however, there was no clear evidence for this assumption. In our study, it was found that the XRD pattern for the original precipitates was not CeO_2 or CeO_{2-x} [27]. Mean-

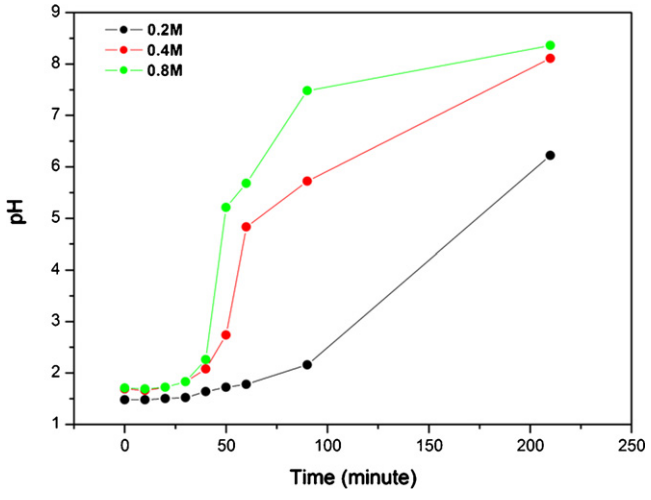

Fig. 1. Time-dependent pH values of the solutions at various concentrations of urea during LT-hydrothermal process.

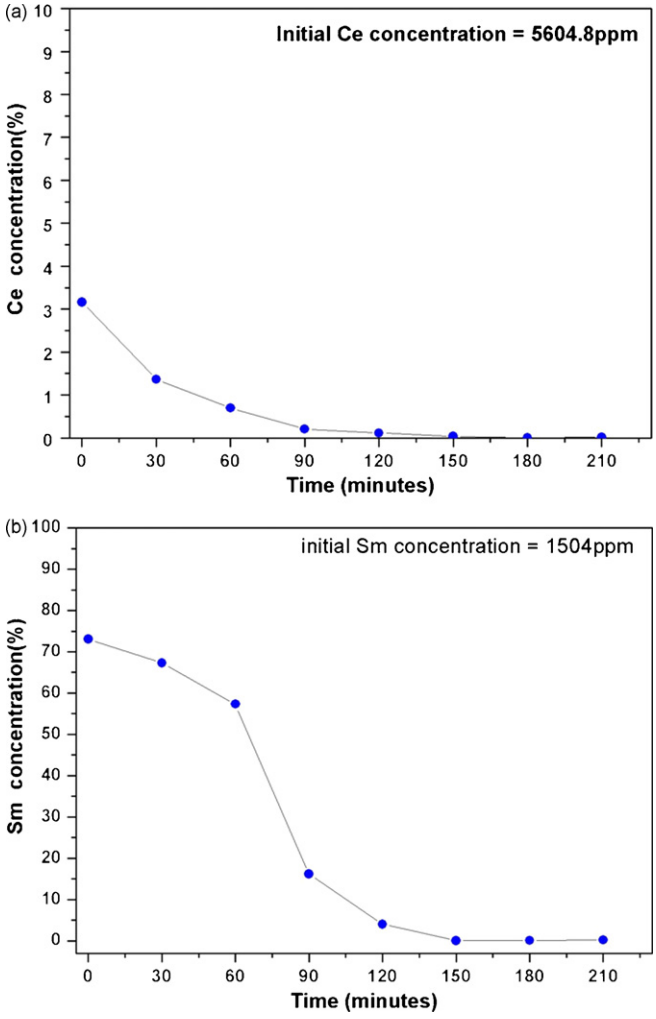

Fig. 2. Time-resolved ICP-AES analysis for (a) Ce^{4+} concentration and (b) Sm^{3+} concentration of the solution at the urea concentration of 0.8 M during LT-hydrothermal process.

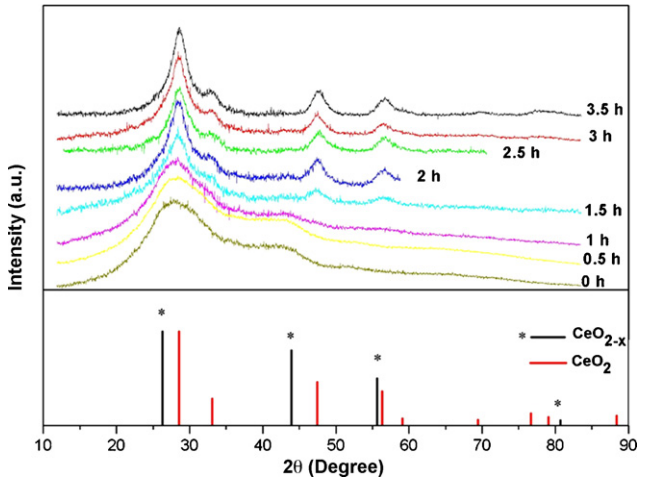

Fig. 3. Time-resolved XRD patterns of the precipitates at the urea concentration of 0.8 M during LT-hydrothermal process.

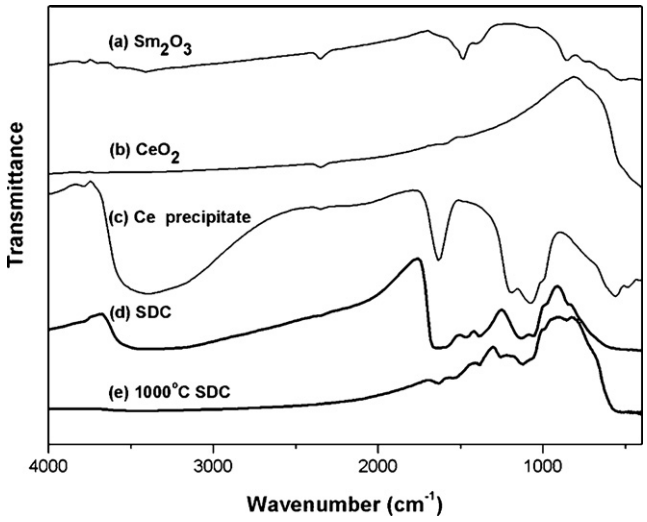

Fig. 4. FTIR spectra of various samples (a) Sm_2O_3, (b)CeO_2, (c) Ce-precipitates, (d) as-synthesized $Ce_{0.8}Sm_{0.2}O_{1.9}$, and (e) 1000 °C-treated $Ce_{0.8}Sm_{0.2}O_{1.9}$.

while, the composition of the precipitates has been confirmed to be cerium-based materials with minor samarium incorporation from ICP-AES analysis. Therefore it can be concluded that the composition of the initial precipitates would be in the form of $Ce_xSm_y(OH)_{4x+3y}$. Although the concentration of Sm^{3+} ions in the solution was reduced rapidly after 1 h, no peaks for $Sm(OH)_3$ or Sm_2O_3 were observed. It was reasonable that the nucleation of $Sm(OH)_3$ was uniform on the surface of the initial precipitates. Meanwhile, the initial precipitates transformed to a cubic fluorite structure after 1.5 h shown in the XRD pattern. It indicated that condensation reaction of the initial precipitates was complete.

The FTIR spectra of (a) commercial Sm_2O_3 powders, (b) commercial CeO_2 powders, (c) original precipitates (formed in the beginning), (d) as-synthesized $Ce_{0.8}Sm_{0.2}O_{1.9}$ nanoparticles and (e) 1000 °C-treated $Ce_{0.8}Sm_{0.2}O_{1.9}$ nanoparticles were shown in Fig. 4. The features of the spectra (a) and (b) were consistent with those of Sm_2O_3 and CeO_2 in the literature [28], respectively. It should be noticed that two characteristic peaks of Fig. 4(a) at 730 and 860 cm^{-1} were identified as the stretching vibration of Sm–O bands [29]. For the spectra of the Ce-precipitates (Fig. 4(c)) and the as-synthesized $Ce_{0.8}Sm_{0.2}O_{1.9}$ nanoparticles (Fig. 4(d)), the prominent peaks at around 3400 and 1640 cm^{-1} were H–O stretching and H–O–H bending vibration, respectively. The shoulder at 2100–2150 cm^{-1} was assigned to water association band. It indicates that water or hydroxyl groups still existed in the Ce-precipitates and as-synthesized $Ce_{0.8}Sm_{0.2}O_{1.9}$ nanoparticles by the evidence of three peaks (1640, 2100–2150 and 3400 cm^{-1}) in the FTIR analysis. Further, it was clear that peaks at 730 and 860 cm^{-1}, which can be taken as the evidence of the incorporation of Sm^{3+} ions into the final precipitates, were only observed in the later one. Moreover, the characteristic peaks of Sm_2O_3 originating from Sm–O band were found in the range of 1250–1500 cm^{-1} of the spectrum (d), indicating Sm oxides or hydroxides exist in the as-synthesized precipitates.

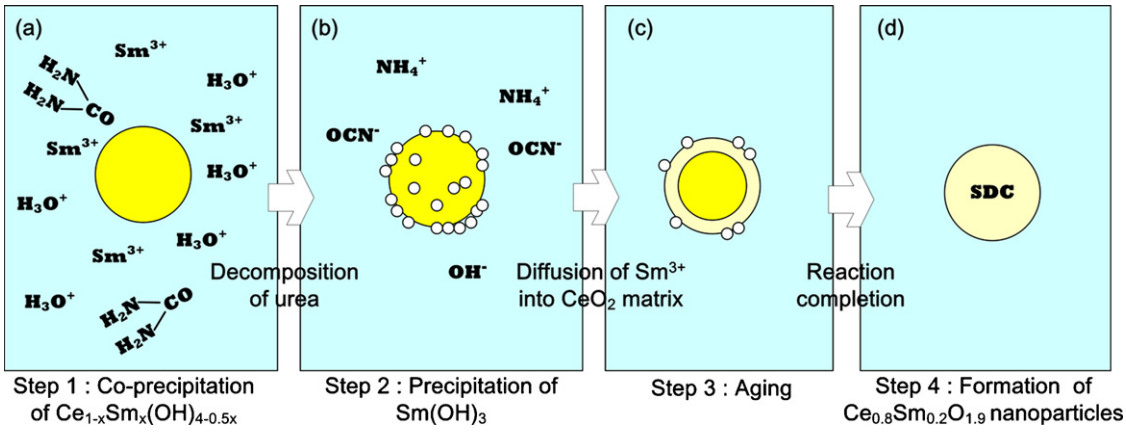

Fig. 5. Proposed formation mechanism of nano-sized $Ce_{0.8}Sm_{0.2}O_{1.9}$ particles prepared by the urea-based LT-hydrothermal process.

Comparing Fig. 4(d) and 4(e), the feature of the 1000 °C-treated synthesized $Ce_{0.8}Sm_{0.2}O_{1.9}$ was almost the same as that of the as-synthesized one except for disappearance of peaks at 1640, 2100–2150 and 3400 cm^{-1}. The absence of these peaks results from the loss of water or hydroxyl groups by the heat treatment.

To determine the lattice parameters of $Ce_{0.8}Sm_{0.2}O_{1.9}$ nanoparticles, XRD patterns were recorded from the synthesized materials mixed with Si powders for calibration. It was found that the lattice parameter expanded obviously ($a = 5.444$ Å) compared to that of the pure CeO_2 ($a = 5.411$ Å, PDF no.: 75-0120) and close to that of JCPDS-ICDD file ($Ce_{0.8}Sm_{0.2}O_{1.9}$, $a = 5.45$ Å, PDF no.: 75-0160). It indicated that Sm^{3+} ions were indeed incorporated into the CeO_2 matrix to form the $Ce_{0.8}Sm_{0.2}O_{1.9}$ solid solution (Sm^{3+}: 1.098 Å, Ce^{4+}: 1.010 Å).

Based on the time-dependent pH value of the solution, composition of the solution and the ex situ XRD analysis of the precipitates, the formation mechanism of $Ce_{0.8}Sm_{0.2}O_{1.9}$ was proposed and shown in Fig. 5. At the early stage, the initial precipitates were believed to be the mixture of cerium and samarium hydroxides via the co-precipitation of Ce^{4+} ions in major and Sm^{3+} ions in minor (step 1). Further, the extensive precipitation of samarium ions occurred after the incubation period (step 2). No other peak in the XRD pattern was referred to the crystalline structure of individual samarium hydroxides after the precipitation of samarium ions. It was proposed to form small $Sm(OH)_3$ clusters on the surface of the initial precipitates. The core–shell-like particles with cerium hydroxide-rich in core and samarium hydroxide-rich in shell formed at this stage. Samarium hydroxides in the shell diffuse into the cerium-rich core in step 3. The doping process was proposed to be caused by diffusion of the samarium from the samarium-rich shell into the defects of the cerium-rich core hydroxides. The formation of the cubic fluorite $Ce_{0.8}Sm_{0.2}O_{1.9}$ crystalline structure was caused by full condensation of the mixed hydroxide (step 4).

TEM image of the synthesized $Ce_{0.8}Sm_{0.2}O_{1.9}$ nanoparticles was shown in Fig. 6. The spherical and nano-sized grains with highly uniform distribution were observed, indicating the advantages of the LT-hydrothermal route. From the images, it was clear that the grain sizes of the nanoparticles were around 3 nm. In Fig. 7, the average grain sizes of the synthesized materials calculated by Scherrer equation with FWHM (full width at half maximum) of the XRD patterns were shown. It was obvious that the grain size of the synthesized materials decreased dramatically when the urea concentration in the solution increased from 0.2 to 0.6 M. However, the size almost remained unchanged for urea concentration higher than 0.6 M. Basically speaking, grain

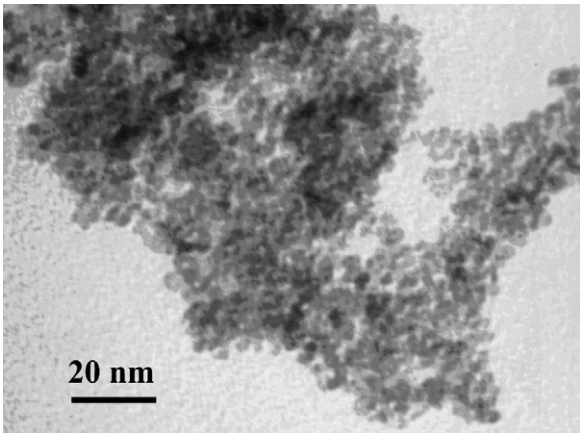

Fig. 6. TEM image of the as-synthesized $Ce_{0.8}Sm_{0.2}O_{1.9}$ nanoparticles.

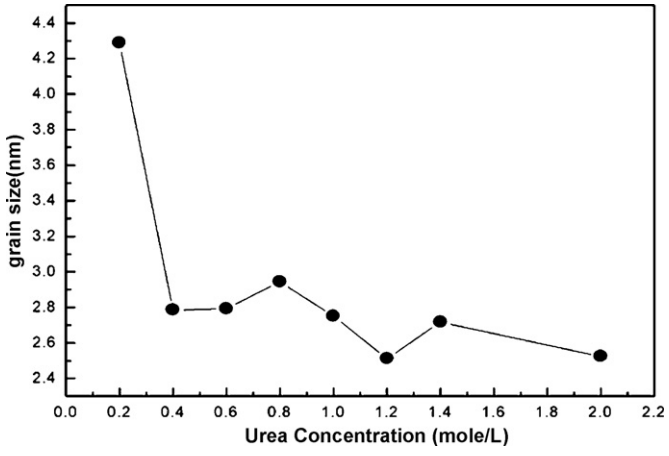

Fig. 7. Calculated grain sizes of the as-synthesized $Ce_{0.8}Sm_{0.2}O_{1.9}$ nanoparticles.

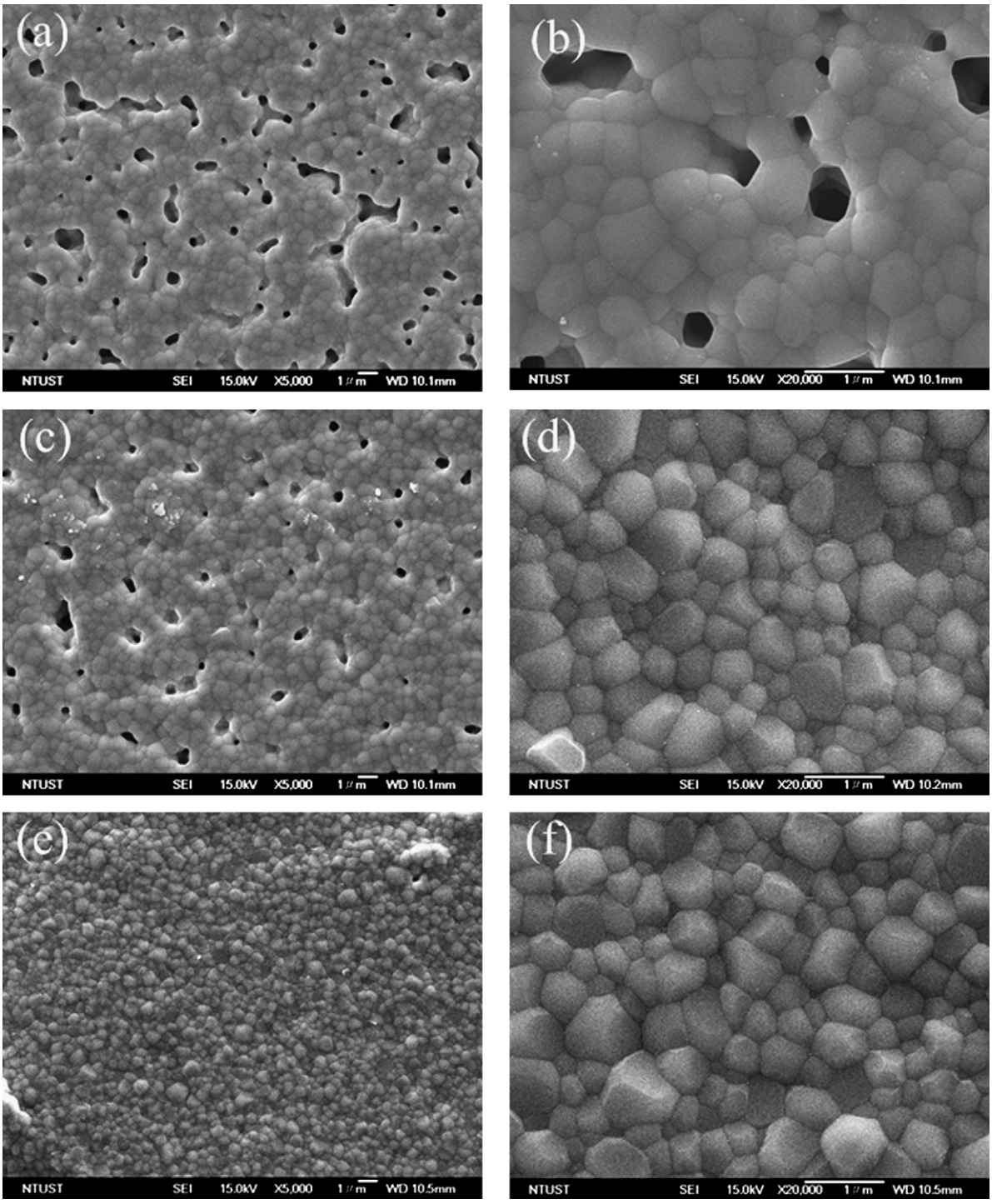

Fig. 8. SEM morphologies of the 1400 °C-sintered SDC disks prepared by the synthesized $Ce_{0.8}Sm_{0.2}O_{1.9}$ nanoparticles at various urea concentrations: 0.4 M: (a) 5000× and (b) 20,000×; 0.8 M: (c) 5000× and (d) 20,000×; or 1 M: (e) 5000× and (f) 20,000×.

size strongly depends on the formation of the nuclei formed at the very early stage. If the amounts of the nuclei decrease, the number and the size of the final produced particles decreased and increased, respectively. In our study, the number of the nuclei is relevant to the concentration of urea in the solution. When the urea concentration is high, the number of the formed nuclei at the very early stage increases. However, if the concentration of the nuclei is too high, the formed nuclei start to aggregate. It is suggested that the concentration of the nuclei formed at the solution containing 0.4 M urea reaches the critical value at the early stage of the hydrothermal process. Thus, the size of the synthesized $Ce_{0.8}Sm_{0.2}O_{1.9}$ nanoparticles was almost unchanged with the solution containing 0.4 M urea or higher concentrations.

The disks made of the $Ce_{0.8}Sm_{0.2}O_{1.9}$ nanoparticles synthesized at different urea concentrations were sintered at 1400 °C for 5 h. The surface morphologies of the sintered disks were

observed by FESEM and shown in Fig. 8. The images showed that the porosity of the sintered disks decreased with an increase of urea concentration and the size distribution of the grains in the disks was quite uniform. According to Ostwald ripening process, heat treatment of the materials with uniform distribution in grain size should result in uniform grain growth. It again supports the advantage of the urea-based LT-hydrothermal method. It was found that the grain size of the sintered samples was independent of urea concentration in the range of 0.6–1.0 M. This is consistent with the line broadening analysis of the XRD data. Although the grain size is similar for the samples prepared at the urea concentration of 0.4, 0.8 and 1.0 M, the porosity of the sintered samples decreases with urea concentration. The TGA measurements have been performed for the SDC powders prepared at the urea concentration of 0.4 and 1.0 M, as shown in Fig. 9. From the TGA results, the SDC powders synthesized at low-urea concentration (0.4 M) shows considerable weight loss after 700 °C. However, the SDC powders synthesized at urea concentration of 1 M exhibits no obvious weight loss after 700 °C. To understand the reason for this difference, the TGA analysis for the precursor of $Ce(SO_4)_2{\cdot}4H_2O$ was also performed. During heating of $Ce(SO_4)_2{\cdot}4H_2O$, crystalline H_2O molecules would vaporize first, followed by the decomposition of SO_4^{2-} anions. Before 340 °C, the weight loss for $Ce(SO_4)_2{\cdot}4H_2O$ is around 17.8 wt.%, almost the same as the weight ratio of the water content in $Ce(SO_4)_2{\cdot}4H_2O$ (17.8 wt.%). The rest of the weight loss after 340 °C should be attributed to the decomposition of the SO_4^{2-} anions. The data show similar trend of weight loss after 700 °C for the SDC powders synthesized at the urea concentration of 0.4 M, indicating the incorporation of SO_4^{2-} anions takes place during the process. It is suggested that the existence of the SO_4^{2-} anions in the SDC powders is responsible for the low-density SDC disk due to the decomposition of SO_4^{2-} anions during sintering process. The relative densities of the disks prepared by the powders synthesized at different urea concentrations were listed in Table 1. It was apparent that the relative density increased with an increase in urea concentration. It was consistent with the observation from the SEM images.

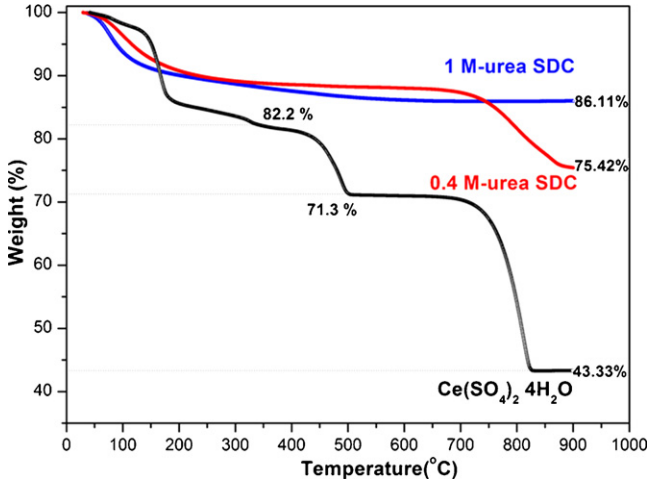

Fig. 9. TGA of $Ce(SO_4){\cdot}4H_2O$ and the synthesized SDC powders prepared at various urea concentrations.

Table 1
Relative density of the sintered-SDC disks

Urea concentration (M)	Relative density (%)
0.4	87.7
0.8	92.7
1.0	99.9

4. Conclusions

The $Ce_{0.8}Sm_{0.2}O_{1.9}$ nanoparticles with unifrom particle size distribution have been successfully synthesized by the developed low-temperature hydrothermal route. The formation mechanism of the developed route for the desired cubic-fluorite structure has been proposed. During the process, the cerium hydroxide-rich precipitates formed at the early stage. Then samarium hydroxides precipitated on the surface of cerium hydroxide-rich precipitates, the core–shell nanoparticles with cerium hydroxide-rich in core and samarium hydroxides-rich in shell were formed and the cerium-rich core was transformed to cubic fluorite structure. Further aging the solution, samarium was incorporated into the cerium oxide-rich core. The formation of $Ce_{0.8}Sm_{0.2}O_{1.9}$ crystalline structure was evidenced by the expansion of lattice constant. In addition, it was found that the sintering ability of the synthesized $Ce_{0.8}Sm_{0.2}O_{1.9}$ increases with urea concentration in the process, which is possibly resulted from the degree of dehydration of the powders during the sintering process. The developed process is easily controlled and reproducible, which could be also applied to other systems where doped oxide nanoparticles are desired.

Acknowledgements

The financial supports from the National Science Council (under contract numbers NSC93-2214-E-011-002, NSC93-2811-E-011-008, NSC94-2214-E-011-010, and NSC94-2120-M-011-002), the National Synchrotron Radiation Research Center (NSRRC), and the National Taiwan University of Science and Technology, Taiwan, ROC are gratefully acknowledged.

References

[1] J.A. Wang, J.M. Dominguez, A. Montoya, S. Castillo, J. Navarrete, M. Moran-Pineda, J. Reyes-Gasga, X. Bokhimi, Chem. Mater. 14 (2002) 4676.
[2] B. Skårman, T. Nakayama, D. Grandjean, R.E. Benfield, E. Olsson, K. Niihara, L.R. Wallenberg, Chem. Mater. 14 (2002) 3686.
[3] P. Shuk, M. Greenblatt, M. Crofe, Chem. Mater. 11 (1999) 473.
[4] F. Bondioli, A.B. Corradi, T. Manfredini, Chem. Mater. 12 (2000) 324.
[5] K. Eguchi, J. Alloys Compd. 250 (1997) 486.
[6] T. Inoue, T. Setoguchi, K. Eguchi, H. Arai, Solid State Ionics 35 (1989) 285.
[7] H. Yahiro, Y. Baba, K. Eguchi, H. Arai, J. Electrochem. Soc. 135 (1988) 2077.
[8] G.A. Tompsett, N.M. Sammes, O. Yamamoto, J. Am. Ceram. Soc. 80 (1997) 181.
[9] M. Mogensen, N.M. Sammes, G.A. Tompsett, Solid State Ionics 129 (2000) 63.
[10] K. Eguchi, T. Setoguchi, T. Inoue, H. Arai, Solid State Ionics 52 (1992) 165.

[11] T. Hibino, A. Hashimoto, T. Inoue, J.I. Tokuno, S.I. Yoshida, M. Sano, Science 288 (2000) 2031.
[12] M. Sahibzada, B.C.H. Steele, K. Zheng, R.A. Rudkin, I.S. Metcalfe, Catal. Today 38 (1997) 459.
[13] T. Tsai, S.A. Barnett, J. Electrochem. Soc. 145 (1998) 1696.
[14] H. Yahiro, Y. Baha, K. Eguchi, H. Arai, J. Electrochem. Soc. 135 (1988) 2077.
[15] H. Yahiro, Y. Eguchi, K. Eguchi, H. Arai, J. Appl. Electrochem. 18 (1988) 527.
[16] B. Hungria, A. Martínez-Arias, M. Fernández-García, A. Iglesias-Juez, A. Guerrero-Ruiz, J.J. Calvino, J.C. Conesa, J. Soria, Chem. Mater. 15 (2003) 4309.
[17] P. Shuk, M. Greenblatt, Solid State Ionics 116 (1999) 217.
[18] W. Huang, P. Shuk, M. Greenblatt, Solid State Ionics 113–115 (1998) 305.
[19] S. Dikmen, P. Shuk, M. Greenblatt, H. Gocmez, Solid State Sci. 4 (2002) 585.
[20] G. Li, R.L. Smith Jr., H. Inomata, J. Am. Chem. Soc. 123 (2001) 11091.
[21] E. Matijević, W.P. Hsu, J. Colloid Interf. Sci. 118 (1987) 506.
[22] P.L. Chen, I.W. Chen, J. Am. Ceram. Soc. 76 (1993) 1577.
[23] X. Chu, W. Chung, L.D. Schmidt, J. Am. Ceram. Soc. 76 (1993) 2115.
[24] M. Hirano, E. Kato, J. Mater. Sci. Lett. 15 (1996) 1249.
[25] M. Hirano, E. Kato, J. Am. Ceram. Soc. 82 (1999) 786.
[26] M.K. van der Lee, A. Jos van Dillen, J.H. Bitter, K.P. de Jong, J. Am. Chem. Soc. 127 (2005) 13573.
[27] F. Vasiliu, V. Parvulescu, C. Sarbu, J. Mater. Sci. 29 (1994) 2095.
[28] R.A. Nyquist, R.O. Kagel, Infrared Spectra of Inorganic Compounds, Academic Press, New York, 1971.
[29] T. Liu, Y. Zhang, H. Shao, X. Li, Langmuir 19 (2003) 7569.